

CHEMICAL ABUNDANCE DISTRIBUTIONS OF GALACTIC HALOS AND THEIR SATELLITE SYSTEMS IN A Λ CDM UNIVERSE

ANDREEA S. FONT,¹ KATHRYN V. JOHNSTON,¹ JAMES S. BULLOCK,² AND BRANT E. ROBERTSON³

Received 2005 July 1; accepted 2005 October 19

ABSTRACT

We present a cosmologically motivated model for the hierarchical formation of the stellar halo that includes a semianalytic treatment of galactic chemical enrichment coupled to numerical simulations that track the orbital evolution and tidal disruption of satellites. A major motivating factor in this investigation is the observed systematic difference between the chemical abundances of stars in satellite galaxies and those in the Milky Way halo. Specifically, for the same $[\text{Fe}/\text{H}]$ values, stars in neighboring satellite galaxies display significantly lower $[\alpha/\text{Fe}]$ ratios than stars in the halo. We find that the observed chemical abundance patterns are a natural outcome of the process of hierarchical assembly of the Galaxy. This result follows because the stellar halo in this context is built up from satellite galaxies accreted early on (more than 8–9 Gyr ago) and enriched in α -elements produced in Type II supernovae. In contrast, satellites that still survive today are typically accreted late (within the last 4–5 Gyr) with nearly solar $[\alpha/\text{Fe}]$ values as a result of contributions from both Type II and Type Ia supernovae. We use our model to investigate the abundance distribution functions (using both $[\text{Fe}/\text{H}]$ and $[\alpha/\text{Fe}]$ ratios) for stars in the halo and in surviving satellites. Our results suggest that the shapes and peaks in the abundance distribution functions provide a direct probe of the accretion histories of galaxies.

Subject headings: cosmology: theory — galaxies: abundances — galaxies: evolution

1. INTRODUCTION

In the current framework of hierarchical structure formation, large galaxies like the Milky Way are believed to form through the merging of many protogalactic fragments (White & Rees 1978; Searle & Zinn 1978; Blumenthal et al. 1984). The observational evidence in support of this model continues to mount, ranging from signatures of different accretion events in the kinematics of globular clusters and halo stars (see Majewski 1993 for an extensive review of the kinematical evidence), to the direct detection of satellite galaxies in the full process of disruption (e.g., the Sagittarius galaxy; Ibata et al. 1994, 1995).

Chemical abundances are an additional rich reservoir of information that can help uncover the formation of the Galaxy (Freeman & Bland-Hawthorn 2002). In their chemical abundances stars retain information about past star formation events and the time of accretion of the halo progenitors from which they came, even in cases when this information is lost in their phase-space distribution due to phase mixing and violent relaxation. Thus, in reconstructing the history of the Galaxy, chemical data complement and enhance the spatial and kinematic data.

Some chemical abundance data are suggestive of past accretion events. For example, stars with kinematics and chemical abundances distinct from the distribution from which they are drawn, whether halo (Carney et al. 1996; Majewski et al. 1996) or disk (Helmi et al. 2006), are likely to originate in recently accreted satellite galaxies. Nissen & Schuster (1997) find that the abundances of α -elements of halo stars decrease with distance in the Galaxy and observe that this may be the result of recent accretions. It is also consistent with the hierarchical scenario that

the kinematics of globular clusters are uncorrelated with their metallicities (Searle 1977).

Other studies raise some concerns about the validity of the hierarchical structure formation scenario. Recent observations have revealed systematic differences in the $[\alpha/\text{Fe}]$ abundances of stars in present-day dwarf spheroidal galaxies (dSphs) and stars in the same $[\text{Fe}/\text{H}]$ range in the halo. Specifically, at metallicities of $[\text{Fe}/\text{H}] \leq -1$, stars in the local halo have above-solar $[\alpha/\text{Fe}]$ ratios ($[\alpha/\text{Fe}] \sim 0.2\text{--}0.4$), whereas stars in the Local Group dwarf galaxies have nearly solar abundances ($[\alpha/\text{Fe}] \sim 0.1$; Fuhrmann 1998; Shetrone et al. 2001, 2003; Venn et al. 2004). The results of these studies show clearly that one cannot assemble an $[\alpha/\text{Fe}]$ -enriched stellar halo from present-day-like satellites that have nearly solar values. The same conclusion can be reached from the study of stellar populations. In trying to relate the young, metal-rich populations in the halo with the contribution from present-day-like dSphs, Unavane et al. (1996) estimate that, at the most, only 6 Fornax-type progenitors or 60 Carinas could have been accreted by the Galaxy. This is in contradiction to the predictions of the hierarchical model, in terms of both the number and the mass spectrum of contributors to a Milky Way-type halo (Unavane et al. 1996; Gilmore & Wyse 1998). Similar discrepancies arise between satellite and halo stellar populations when comparing the abundances of (intermediate age) giant carbon stars in each, with the stellar halo apparently less abundant in these stars than current dwarf satellites (van den Bergh 1994).

However, it is not obvious that the halo progenitors (or, as they are often referred to, the Galactic “building blocks”) were replicas of present-day satellite galaxies. As pointed out by Mateo (1996), present-day dSphs are survivors, and therefore special conditions must have precluded them from disruption (late accretion and/or less-radial orbital characteristics). These conditions could have allowed present-day dSphs to follow a different evolutionary path than the original building blocks. A difference in time of formation alone could explain the lack of intermediate and young populations in the halo relative to the present-day satellites (van den Bergh 1994; Majewski et al. 2002); running back

¹ Van Vleck Observatory, Wesleyan University, Middletown, CT 06459; afont@astro.wesleyan.edu, kvj@astro.wesleyan.edu.

² Department of Physics and Astronomy, University of California, Irvine, CA 92687; bullock@uci.edu.

³ Harvard-Smithsonian Center for Astrophysics, 60 Garden Street, Cambridge, MA 02138; brobertson@cfa.harvard.edu.

the clock to the time when the stellar halo was forming, a Carina-type galaxy would have looked very different.

A true test for hierarchical structure formation needs to use models of satellite galaxy accretions that track their dynamics as well as the development of their stellar populations. Following the chemical evolution of the Galaxy in the full cosmological context is not an easy task, given the current limitations in some of the theoretical areas that need to be covered. In order to tackle this problem, one has to have a model that incorporates a realistic merger history of a Milky Way-type galaxy, a detailed follow-up of the dynamical evolution of substructure inside the galactic potential well, and a chemical evolution model that includes an accurate treatment of stellar yields, the initial mass function, and winds from massive and intermediate-mass stars. We present here one such attempt to model the evolution of the Galaxy. Our approach is a blending of two theoretical methods, the first constructing Milky Way-type stellar halos from accreting substructure (Bullock & Johnston 2005), the second modeling the chemical evolution of individual satellite galaxies by taking into account both the inflow and outflow of matter (Robertson et al. 2005). Both these models individually suggest solutions to the apparent contradiction between observations and the hierarchical structure formation scenario; Bullock & Johnston (2005) show that halo stars were likely to have been accreted much earlier than the surviving satellite population, and Robertson et al. (2005) examine the pattern of chemical abundances in dwarfs with star formation histories truncated at early and late times. This paper extends their study to simultaneously follow both the full phase-space and abundance distributions, allowing us to make definitive statements about the comparison of satellite and halo abundance distributions. Our study follows the phase-space distribution of halo and satellite stars with a higher numerical resolution than previous studies (e.g., Brook et al. 2005) and specifically targeting these galactic components.

In § 2 we outline the main steps of the methods. Section 3 presents the results of mass accretion histories and chemical enrichment of the simulated halos. In § 4 we compare our results with current observations, and in § 5 we conclude.

2. METHODS

2.1. Building Up Stellar Halos through Accretion Events

Throughout this work we assume a Λ CDM universe with $\Omega_m = 0.3$, $\Omega_\Lambda = 0.7$, $h = 0.7$, and $\sigma_8 = 0.9$, in which the Milky Way stellar halo forms entirely from the accretion and disruption of satellite galaxies. Our approach uses a combination of semi-analytic prescriptions and N -body simulations in order to follow the evolution of the phase-space structure of the stellar halo. A brief summary follows (for full details, see Bullock & Johnston 2005).

Mass accretion histories of 20 Milky Way-size galaxies are constructed using the method outlined in Somerville & Kolatt (1999) based on the extended Press-Schechter (EPS) formalism (Lacey & Cole 1993). We select the eleven histories from this sample that do not have significant accretions (that is, individual accretions no more than $\sim 10\%$ of the entire mass of the parent halo) during the past 7 Gyr, similar to the case of the Milky Way (Wyse 2001). For each event in these merger trees, an N -body simulation is generated that follows the dynamical evolution of the accreted satellite's dark matter halo from entry into the main halo up to the present time. During the simulation, the satellite orbits in an analytic disk/bulge/halo potential representing the parent galaxy. The mass and scale of all components of the parent grow with time in proportion to the virial mass and scale of main halo generated by the merger tree.

Each dark matter satellite has a stellar mass that is assigned using a cosmologically motivated analytic formalism. The infall of cold gas into each satellite is followed from the epoch of reionization to the time of its accretion onto the main halo. The gas mass is translated into a stellar mass through a simple star formation prescription (see Robertson et al. 2005 and § 2.2 for more details). Star formation ceases soon after accretion onto the main halo, as it is assumed that the gas is lost at that point due to ram pressure stripping. The free parameters in this model are fully constrained by requiring that it approximately reproduces (1) the number of luminous satellites of the Milky Way, and (2) the ratio of gas to stellar mass in Local Group field dwarfs (which are assumed to correspond to satellites in the model infalling onto the parent today).

The stellar distribution within each satellite is not modeled self-consistently during the N -body simulations; rather, the stars are “painted on” subsequently by assigning a variable mass-to-light ratio to each (equal mass) dark matter particle within a satellite. The stellar profile is assumed to follow a concentration $c = 10$ King model (King 1962), whose extent is set by the observed trend of core radius with luminosity for Local Group dwarfs.

With all possible freedom in the model now constrained, it additionally produces the observed stellar mass-circular velocity (M_*-v_{circ}) relation for Local Group dwarfs (both the amplitude and slope); distributions of surviving satellites in luminosity, central surface brightness, and central velocity dispersion; and stellar halo luminosity and density profile.

2.2. Chemical Evolution of Satellite Galaxies

The chemical enrichment of each satellite galaxy is modeled with the chemical evolution code developed by Robertson et al. (2005), which tracks the evolution of a range of heavy elements, in particular of Fe and α -elements such as Mg, O, Ca, Ti, etc. This model takes into account the enrichment from both Type II and Type Ia supernovae, as well as the feedback provided by supernovae blowout and winds from intermediate-mass stars. Hot gas and metals that are expelled from satellites disperse into the main halo and cannot be later accreted back onto the satellite they originated from. This is a reasonable assumption, since the velocity dispersion of the gas heated by SNe ($\sim 200 \text{ km s}^{-1}$) is generally much larger than that of satellite galaxies (typically, of order $10\text{--}50 \text{ km s}^{-1}$ for dwarf galaxies).

The galactic outflow is assumed to start once the thermal energy of the expelled material (gas or metals) exceeds the gravitational binding energy of the satellite. Since the binding energy per unit mass increases with mass of the galaxy, the wind efficiency is expected to decrease with mass. Hence, the galactic wind is modeled as a function of the depth of the potential well of the satellite galaxy. The normalization of this function is chosen (in conjunction with a star formation timescale) so that the agreement with the observational constraints described in the previous section is maintained (i.e., the M_*-v_{circ} relation, gas-to-stellar-mass ratio of Local Group dwarfs, and the total luminosity of the stellar halo).

It is further assumed that winds are metal enriched, as metals are shown to escape the potential well with greater efficiency than the gas (Mac Low & Ferrara 1999; Ferrara & Tolstoy 2000). The normalizations of the metal (Fe and α -elements) wind efficiencies are treated as parameters. The Fe wind efficiency is constrained by requiring a match to the stellar mass-metallicity (M_*-Z) relation (Larson 1974; Dekel & Silk 1986; Dekel & Woo 2003) over a wide range of dwarf galaxies' masses ($M_* \sim 10^6\text{--}10^9 M_\odot$; see also Mateo 1998 and references therein), while the α -element wind efficiency is chosen to reproduce the chemical abundance patterns of stars in dSph satellites (Venn et al. 2004).

TABLE 1
PROPERTIES OF THE FOUR SIMULATED HALOS AND THEIR SATELLITES

Halo	Stellar Halo Luminosity ($10^9 L_{\odot}$)	Number of Satellites (Dark Matter/Baryonic)	Number of Surviving Baryonic Satellites
H1.....	1.75	391/113	18
H2.....	1.64	373/102	6
H3.....	1.40	322/104	16
H4.....	1.90	347/97	8

Since gas and hence star formation in satellites is truncated upon accretion in our model, it will not reproduce any recent significant star formation or chemical enrichment histories of the few surviving gas-rich systems like the LMC and SMC, for which extended chemical modeling may be needed (Recchi et al. 2001). It also may not be applicable to spiral satellite galaxies, in which case it is believed that the regulatory factor in the M_* - Z relation is not the galactic winds but a prolonged star formation (Tosi et al. 1998; Matteucci 2001, pp. 145–147). However, it should reasonably represent dSphs, since these systems do not have a significant amount of gas or significant star formation at the present day (Mateo 1998; Grebel et al. 2003). Although there is evidence for recent star formation in several dSphs (Gallart et al. 1999; Smecker-Hane & McWilliam 1999), our model suggests that these systems are likely to have been accreted relatively recently (see § 3.1), so the majority of their stars are expected to have formed prior to accretion. Moreover, satellites in general disrupt completely (and hence any continuing star formation would be truncated, whether or not gas stripping was efficient) within one or two orbits following their accretion time, so we anticipate that our model will reproduce the bulk of halo stars (see § 4.1 for further discussion of this point).

2.3. Tracking the Combined Chemical Abundances and Phase-Space Distribution

Using the methods outlined in § 2.2, we assign each satellite a unique set of stellar populations dictated by its own cosmologically motivated mass accretion history, which in turn determines its star formation history and subsequent chemical evolution. We then give each star particle in the satellite a set of chemical abundances ($[\text{Fe}/\text{H}]$ and $[\alpha/\text{Fe}]$) drawn at random from the stellar populations. In doing so, we assume that all heavy elements are homogeneously mixed within each satellite. This assumption is rather simplifying, as heavy elements may be spatially segregated (see observations by Tolstoy et al. 2004). However, the still-limited information about possible metallicity gradients in satellite galaxies precludes us from adopting a more sophisticated model for the metallicity spatial distributions.

We now have full phase-space, luminosity, and metallicity information for stellar material associated with all the accretion events in our merger trees and can examine the resulting spatial and kinematic distribution of metals in our stellar halos and their surviving satellites systems. Below we present results of a sample of four such simulated galaxy halos, specifically, halos 1–4 from the 11 simulated halos discussed in Bullock & Johnston (2005). We denote them as halos H1, H2, H3, and H4. Table 1 describes the properties of these four halos such as the total halo luminosity,⁴

number of dark and luminous satellites, and the number of satellites that survive until the present day.

3. RESULTS

We describe below the mass accretion histories of the simulated galaxy halos (§§ 3.1 and 3.2) and the resulting chemical abundances of both surviving satellites and stellar halo (§ 3.3). We then discuss the chemical abundance variations between different halo components as well as between different halo realizations (§ 3.4).

3.1. Accretion Times of Stellar Halos and of Surviving Satellites

An important question in understanding the formation of the Galaxy is whether the stellar halo followed the same pattern as that of the dark matter halo. The hierarchical assembly of galaxy halos is expected to result in a distinctive inside out growth pattern for the dark matter. Some inferences about the growth of the stellar component of galaxy halos have been made based on scaled-down versions of cluster simulations and by assuming physically motivated properties for the baryonic material (Zhao et al. 2003; Helmi et al. 2003). Recently, simulations targeted specifically to model of stellar galaxy halos confirm that these too form inside-out in a short period of time, on the order of a few Gyr (Bullock & Johnston 2005).

Here we investigate the accretion history of different regions of the stellar halo, with the aim of identifying which satellites are the dominant contributors and what their characteristics are. This will be important when assessing the buildup of halo chemical abundances, since these retain the signature of the satellite galaxies from which they originate.

Figure 1 shows the stellar mass accretion history of each halo binned in time intervals of 0.2 Gyr (here t_{accr} denotes the look-back time of accretion, $t = 0$ corresponds to the present time). The top row of panels describes the buildup of the entire halo, while the rows below show the buildup of the inner ($R < 20$ kpc), intermediate ($20 \text{ kpc} < R < 50$ kpc) and outer ($50 \text{ kpc} < R < 100$ kpc) parts of the stellar halo, respectively. All regions are centered around the solar neighborhood (i.e., R is the distance relative to the position of the Sun at $R_{\odot} = 8.5$ kpc from the Galactic center in the disk). Filled histograms represent the stellar material still gravitationally bound to a surviving satellite at $t = 0$, and open histograms represent the entire accreted stellar mass (both disrupted and still gravitationally bound). The inner halo region in the simulations is the counterpart of the “local halo” typically accessible in observations. The figure shows that this region assembles early on. For example, $\sim 80\%$ of all inner halos (indicated by arrows in the second row panels) are already in place by look-back time ~ 8 – 9 Gyr. The bulk ($\sim 80\%$) of the intermediate and outer regions form at roughly the same time as the inner one, however these regions have a slightly larger stellar fraction added at later times ($10 \text{ Gyr} < t_{\text{accr}} < 5 \text{ Gyr}$) than the inner one. The material still bound today (i.e., residing in surviving satellites) has been accreted more recently, generally within the past

⁴ Note that the halo luminosities are slightly different from the values quoted by Bullock & Johnston (2005). The differences arise from the different treatment of the star formation rate (i.e., whether feedback is modeled explicitly, as in this paper, or implicitly, as in Bullock & Johnston 2005).

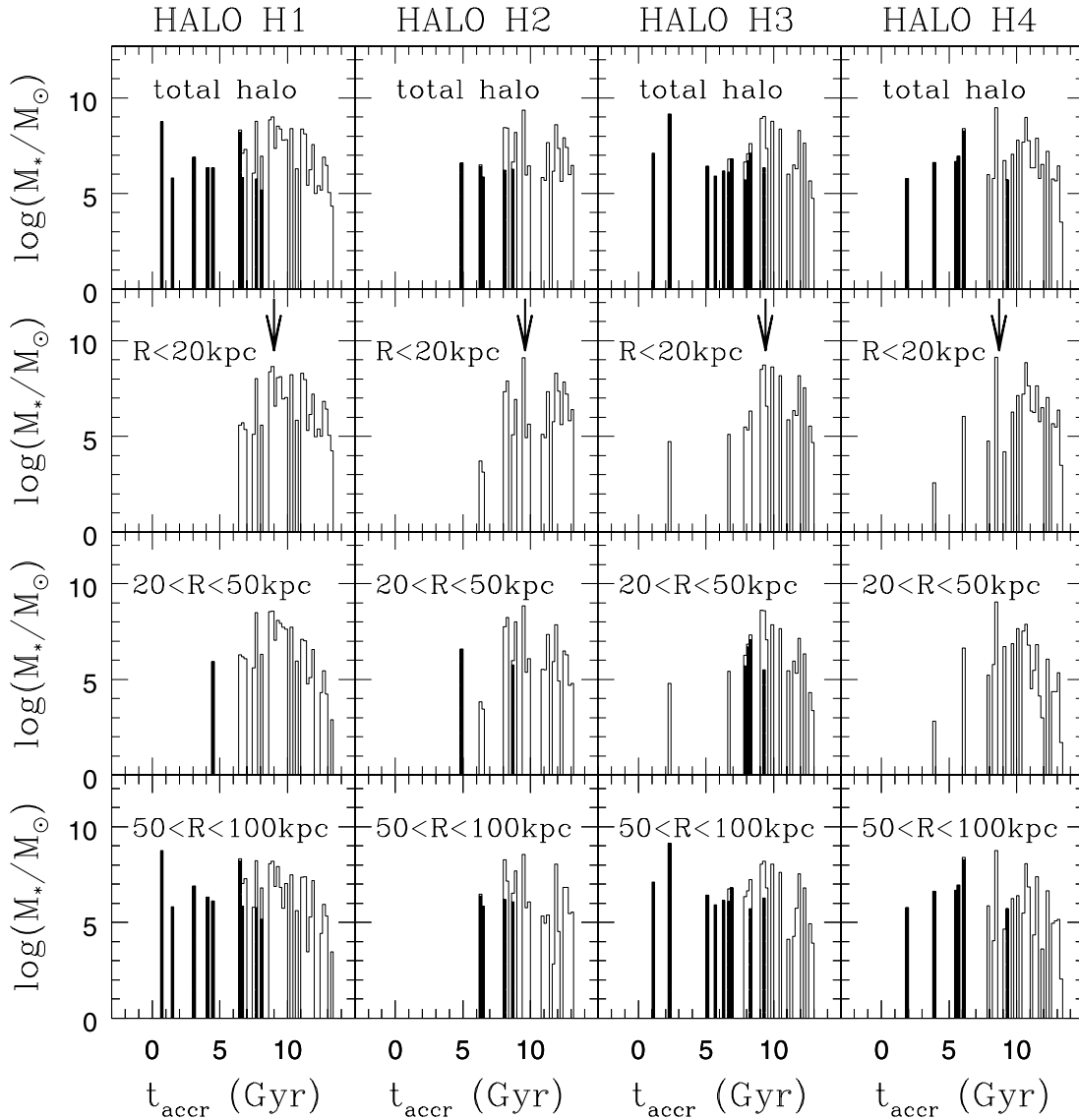


FIG. 1.—Mass accretion histories of the four simulated halos. The histograms represent the accreted mass that is deposited in the entire halo (*top row*); in the inner halo, $R < 20$ kpc (*second row*); in the intermediate halo, $20 \text{ kpc} < R < 50$ kpc (*third row*); and in the outer halo, $50 \text{ kpc} < R < 100$ kpc (*bottom row*), respectively. Here R is the distance relative to the position of the Sun, $R_{\odot} = 8.5$ kpc. The open histograms represent the entire mass (both bound and unbound) accreted in the corresponding distance interval and the filled histograms represent the material that is still gravitationally bound at $t = 0$. The arrows in the second row panels correspond to the times when 80% of the inner halo has formed in each run.

5–6 Gyr. None of the surviving satellites are located in the inner $R < 20$ kpc of the halo, where tidal forces are strongest. This result is in agreement with the location of present-day Local Group dwarf galaxies, which tend to reside at large distances from the center of the potential well (Mateo 1998); the single exception is the Sagittarius galaxy, which is in the process of being disrupted.

Both the time of accretion and orbital parameters are expected to determine the chances for survival for infalling substructure. Figure 2 shows the accretion times, t_{accr} , and orbital circularities, ϵ , for baryonic satellites of all four halos superimposed. The orbital circularity ϵ is defined as the ratio of the angular momentum of the orbit of the satellite, J , to that of an equivalent circular orbit of the same energy, J_{circ} . Open squares denote satellites fully disrupted and filled hexagons, satellites that are either intact or that still retain some bound material at the present time. The figure suggests a consistent pattern for all halos; satellites accreted early, $t_{\text{accr}} > 9$ Gyr, are fully disrupted by the tidal field, regardless of their orbital characteristics. Satellites accreted at interme-

mediate look-back times, $5 \text{ Gyr} < t_{\text{accr}} < 9$ Gyr, are more likely to survive if they are on or near circular orbits ($\epsilon \rightarrow 1$). All satellites accreted within the past 5 Gyr survive. Applying our results to present-day satellite galaxies of the Milky Way, we can infer that these are likely to have been accreted less than 8–9 Gyr ago.

Our results suggest that present-day satellites had more time available for sustaining star formation and hence further their chemical enrichment compared to local halo progenitors. Hence, differences in chemical abundances between infalling substructures might be expected.

3.2. Mass Accretion Histories

We further investigate the relative contribution of different satellites to the stellar halo. Is the halo made up mainly by a few massive satellites or by a multitude of smaller ones? Figure 3 shows the fraction of the stellar halo f_* contributed by each disrupting satellite of stellar mass M_* , either binned in mass intervals $\Delta \log(M_*/M_{\odot}) = 0.5$ (*histograms*) or by individual contributions

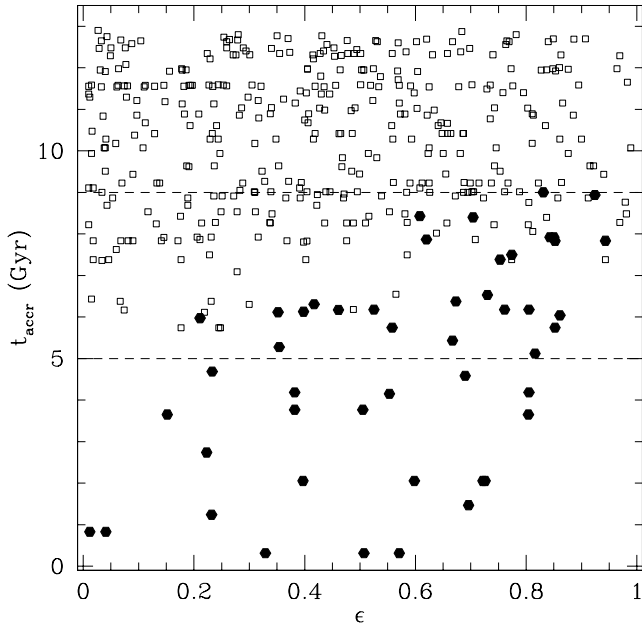


FIG. 2.—Time of accretion t_{accr} , vs. orbital circularity ϵ , plotted superimposed for all satellites of the four simulated halos. Satellites totally disrupted at $t = 0$ are plotted with open squares, and those that still have some bound mass at the same time are filled hexagons. Satellites tend to have more chances to survive if they are accreted late (look-back time $t_{\text{accr}} \leq 9$ Gyr) and are on relatively circular orbits (circularity $\epsilon \rightarrow 1$).

(symbols). Solid lines and filled squares correspond to the entire stellar halo, and dashed lines and open circles correspond to the inner halo. This figure shows that, in terms of stellar mass, a few massive satellites contribute the most to both the inner and the total halo. One or a few more satellites in the range $M_* \sim 10^8 - 10^{10} M_\odot$ can make up 50%–80% of the stellar halo. These results are in agreement with results of previous studies that found that most of the dark matter halo is made up of a few massive, $M \sim 1 - 10 \times 10^{10} M_\odot$, (dark matter) subhalos (Zentner & Bullock 2003; Helmi et al. 2003), or that the properties of the present-day population of globular clusters are consistent with most of these clusters originating in a few massive halo progenitors (Coté et al. 2000).

3.3. Chemical Abundances in the Stellar Halo and Surviving Satellites

The link between the mass accretion histories and the chemical abundances of satellites for the four simulated halos is analyzed in Figure 4. The top panels for each halo show the distribution of average $[\text{Fe}/\text{H}]$ values (averages are weighted by the contribution of different stellar populations) versus stellar mass of satellites, M_* . The different symbols separate satellites in terms of their accretion time; blue squares denote satellites accreted at look-back time $t_{\text{accr}} > 9$ Gyr, green triangles represent those with $5 \text{ Gyr} < t_{\text{accr}} < 9$ Gyr, and magenta pentagons are used for satellites accreted less than 5 Gyr ago. The dashed lines in each top panel correspond to the stellar mass–metallicity fit derived by Dekel & Woo (2003) based on Local Group dwarf data, confirming the agreement.

Figure 4 shows that there are many satellite galaxies accreted at early times with a wide range of $[\text{Fe}/\text{H}]$, including a few massive ones, $M_* > 10^9 M_\odot$. Satellites accreted later have intermediate or large masses and generally larger average $[\text{Fe}/\text{H}]$ values. This is to be expected, since both M_* and $[\text{Fe}/\text{H}]$ increase monotonically with star formation. The middle panels repeat the

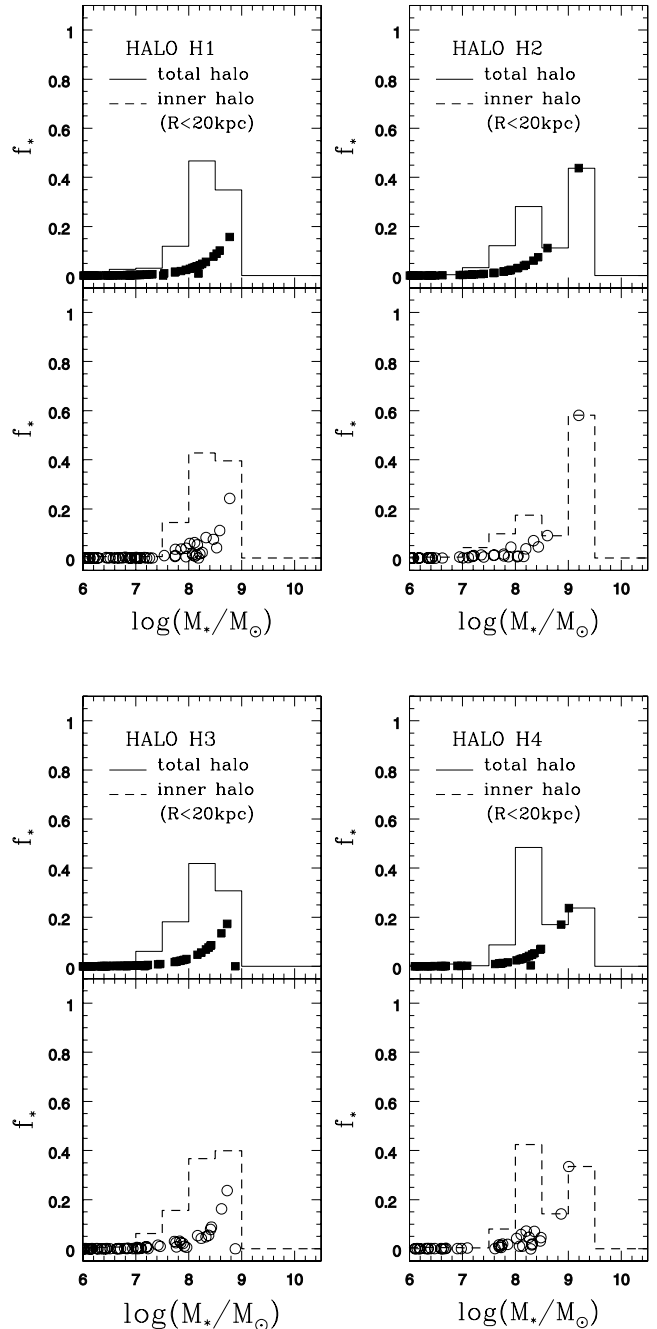


FIG. 3.—Stellar fraction f_* of the halo vs. stellar mass M_* of the contributing satellites. Solid lines and filled squares correspond to the satellites contributing to the total halo and the dashed lines and open circles to those that contribute to the inner halo.

stellar mass– $[\text{Fe}/\text{H}]$ data, this time emphasizing whether satellites are fully disrupted (triangles) or still retain some bound material at $t = 0$ (hexagons). This shows that surviving satellites generally have larger average $[\text{Fe}/\text{H}]$ values, as might be expected from their late time of accretion.

The bottom panels show the average $[\alpha/\text{Fe}]$ values (also weighted by the contribution of different stellar populations) versus M_* for all satellites in a given halo. Here α is taken as the average $[(\text{Mg} + \text{O})/2\text{Fe}]$ (this definition will be used hereafter). The figure shows that satellites that still have some bound material at the present time also tend to have lower $[\alpha/\text{Fe}]$ than the disrupted satellites.

We also verify whether the resulting ages of the stellar populations in our simulated halo agree with observations. The top

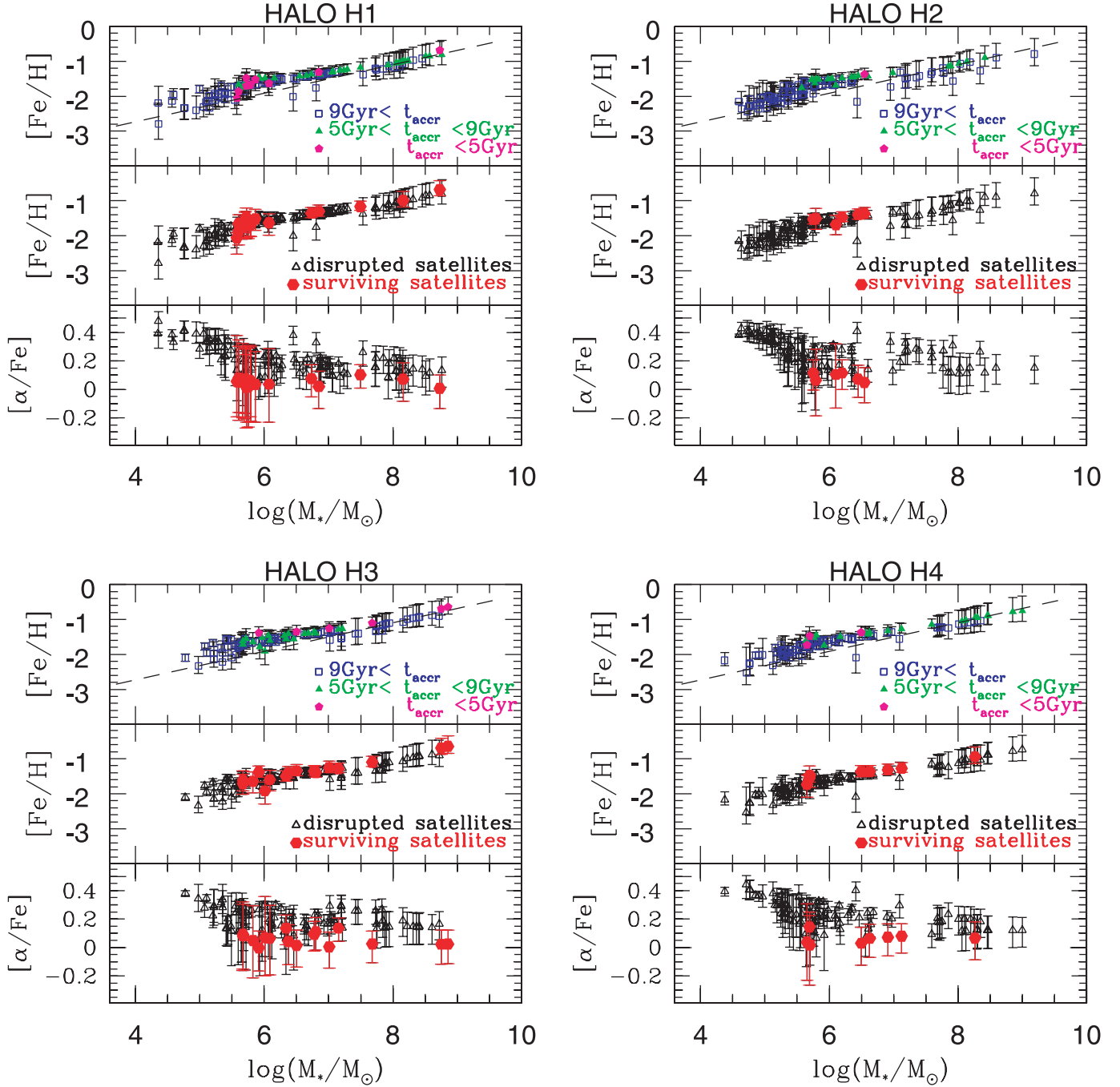


FIG. 4.—Chemical abundance patterns for the satellite distribution in the simulated halos. Each panel corresponds to a simulated halo and contains three subpanels. The top subpanel illustrates average $[\text{Fe}/\text{H}]$ values vs. stellar mass, M_* , color coded in terms of their time of accretion, blue squares for satellites accreted at look-back time $t_{\text{accr}} > 9$ Gyr, green triangles for satellites with $5 \text{ Gyr} < t_{\text{accr}} < 9$ Gyr, and magenta pentagons for satellites accreted less than 5 Gyr ago. The dashed line in each top subpanel corresponds to the Dekel & Woo (2003) relation. The middle subpanel contains the same parameters, this time emphasizing the satellite material still gravitationally bound at $t = 0$ (red hexagons) vs. satellites that are totally disrupted (black triangles). The bottom subpanel shows average $[\alpha/\text{Fe}]$ values vs. M_* for the satellite material still bound at $t = 0$ (red hexagons) and for the satellites that are totally disrupted (black triangles).

panel in Figure 5 shows the age-metallicity relation for all disrupted satellites accreted onto one of the simulated halos (halo H1), plotted as weighted average values. The result is in general agreement with the observed age-metallicity relation in the Milky Way halo (Buser 2000). In the bottom panel we plot the corresponding age distribution of halo stars in the H1 simulation, shown for different look-back time intervals: $t_{\text{accr}} > 9$ Gyr, $5 \text{ Gyr} < t_{\text{accr}} < 9$ Gyr, and $t_{\text{accr}} < 5$ Gyr, respectively. This figure shows that only those satellites accreted recently (within the past ~ 5 Gyr)

contain significant young stellar populations, i.e., with ages less than ~ 5 –7 Gyr.

3.4. Abundance Distribution Functions

The metallicity distribution function (MDF) is frequently used to infer the chemical evolution of galaxies and from this, their formation history. In the following discussion, we analyze both the $[\text{Fe}/\text{H}]$ and $[\alpha/\text{Fe}]$ distribution functions, which from now on will be broadly referred to as “abundance distribution functions” (ADF).

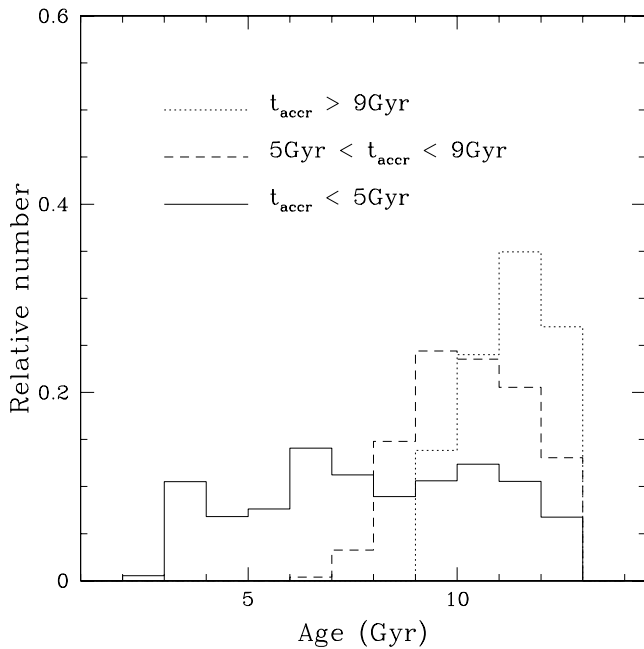
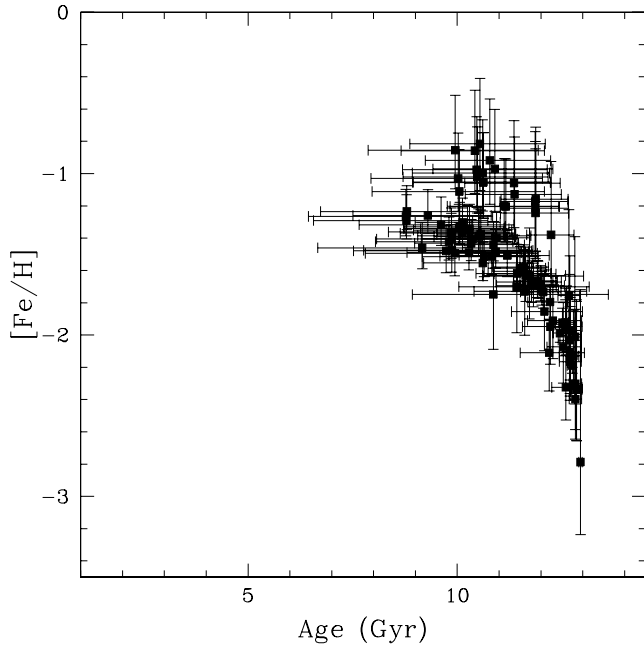


FIG. 5.—*Top*: Age vs. metallicity relation for one of the simulated halos, Halo H1. The data points represent weighted averages for all satellites with error bars spanning from 10% to 90% of these values. *Bottom*: The age distribution of halo stars accreted more than 9 Gyr ago, between 5 and 9 Gyr ago, and within the last 5 Gyr. The histograms are normalized to each distribution.

Figure 6 shows a comparison between the $[\text{Fe}/\text{H}]$ distribution function of the surviving satellites (*dashed lines*) and that of the inner halos (*solid lines*) in our set of four simulations. The MDF peaks of the inner stellar halos range from $\simeq -1$ (halos H1, H3, and H4) to $\simeq -0.6$ (halo H2). The $[\text{Fe}/\text{H}]$ distributions of satellite stars are typically narrower than the corresponding distributions of the inner halos and they too, show a range in their peaks from $\simeq -1.4$ (halo H2) to -0.4 (halo H3).

The differences in the location of the MDF peaks in the four simulations arise from the different halo mass accretion histories. For example, most of the surviving satellites in the H2 run have been accreted earlier than the corresponding surviving satellites

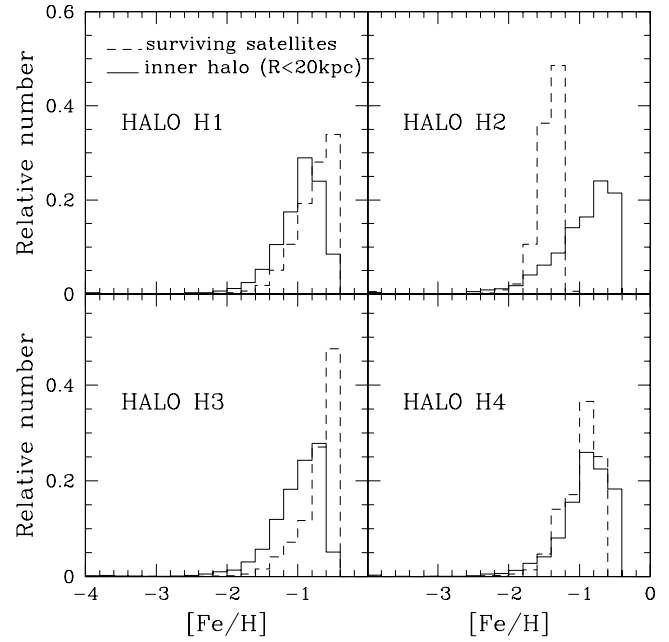


FIG. 6.— $[\text{Fe}/\text{H}]$ distribution functions of stars in the inner halo (*solid line*) and of stars in surviving satellites (*dashed lines*) for the four simulations.

in other runs (see Fig. 1), and have low masses, and hence relatively low $[\text{Fe}/\text{H}]$ values (see Fig. 4). Therefore, the surviving satellites' $[\text{Fe}/\text{H}]$ peak is shifted toward the more metal-poor end. On the other hand, most of the contribution to the inner H2 halo MDF is made by as single massive satellite, $M_* \simeq 10^9 M_\odot$ (see Fig. 3), whereas a significant fraction of the H1 and H3 inner halos is added by numerous smaller satellites. This implies a shift in the $[\text{Fe}/\text{H}]$ distribution peak toward the more metal-poor values in halos H1 and H3 than in H2. The H4 run is the only one with similar $[\text{Fe}/\text{H}]$ distributions in the inner halo and in surviving satellites, which is the result of a balanced contribution to the halo stellar fraction from both low- and high-mass satellites

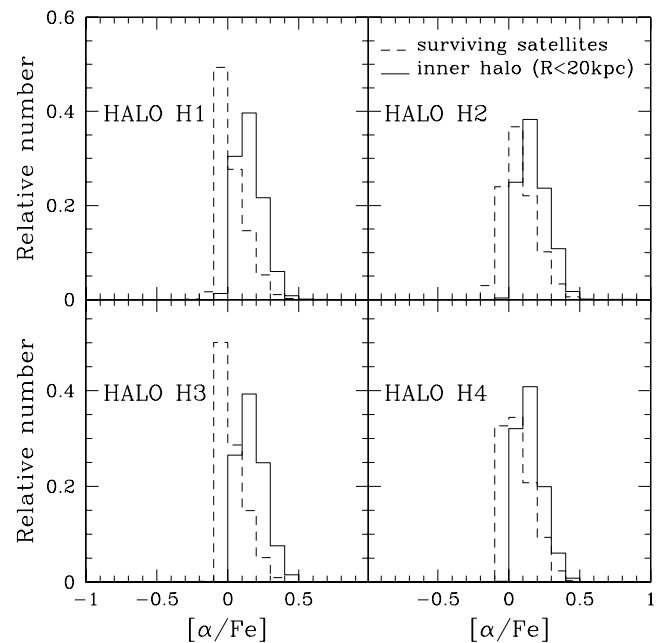


FIG. 7.— $[\alpha/\text{Fe}]$ distribution functions of the stars in the inner halo (*solid line*) and those in surviving satellites (*dashed line*) for the four simulations.

(see Fig. 3) and from an average mass range of the surviving satellites, $M_* \simeq 10^8\text{--}10^9 M_\odot$ (see Fig. 1).

Figure 7 shows a similar histogram for the $[\alpha/\text{Fe}]$ data. As for $[\text{Fe}/\text{H}]$, the $[\alpha/\text{Fe}]$ distribution of satellite stars is narrower than the corresponding distribution of the inner halo, and generally shows a systematic offset. The spread within the $[\alpha/\text{Fe}]$ distribution function seems to be consistently smaller than the spread in the $[\text{Fe}/\text{H}]$ distribution function for both surviving satellites and the inner halo.

4. DISCUSSION

4.1. Comparing the Milky Way and Simulated Chemical Abundance Patterns.

How do our Milky Way–type halos fare in comparison with the Milky Way data? Figure 8 shows the $[\text{Mg}/\text{Fe}]$ versus $[\text{Fe}/\text{H}]$ from the compilation data⁵ of Venn et al. (2004 see references therein for information about the original data). This sample contains stars from both halo and dwarf galaxies and a wide range of chemical abundance information. We select from this compilation all satellite stars (a total of 36) and all stars with halo membership probabilities greater than 50%, which results in a total of 259 halo stars (compared with 235 halo stars, had we selected all stars with halo membership probability of 100%).

In Figure 9 we plot the $[\text{Mg}/\text{Fe}]$ versus $[\text{Fe}/\text{H}]$ for the simulated local halos and surviving satellites. For the local halo, we use the unbound stellar material binned in $[\text{Fe}/\text{H}] = 0.1$ dex intervals. The values corresponding to the surviving satellites are weighted averages only over the bound material to these systems. Solid lines represent error bars of 10% and 90% of weighted average $[\text{Mg}/\text{Fe}]$ values. Dotted lines highlight the absolute extent in $[\text{Mg}/\text{Fe}]$ values for the inner halo. Figure 9 shows again that stars in surviving satellites have consistently lower $[\text{Mg}/\text{Fe}]$ values than stars in the halo. Although there is some overlap in the $[\text{Mg}/\text{Fe}]$ values, the great majority of halo stars have $[\text{Mg}/\text{Fe}]$ values 0.1–0.4 dex higher than that of present-day satellites.⁶

Our results reproduce the trend of Galactic chemical abundance patterns found in observations and the overall offset in $[\text{Mg}/\text{Fe}]$ (and hence $[\alpha/\text{Fe}]$) ratios between satellites disrupted and surviving dSphs. As also discussed by Robertson et al. (2005), the key factors that influence this offset are the time of accretion and the mass of the satellite contributing to the halo. The $[\alpha/\text{Fe}]$ ratio has been often referred to as a “cosmic clock” of galaxy formation. Based on the time delay of about 1 Gyr between the onset of supernovae Type II (which produce both Fe and α elements) and Type Ia (which produce only Fe), a break in $[\alpha/\text{Fe}]$ ratios of halo stars is expected to occur at intermediate metallicities (around $[\text{Fe}/\text{H}] \simeq -1.0$; e.g., McWilliam 1997). The local halo is built up fast, within the first few Gyr of the lifetime of the galaxy, from dwarf galaxies with high $[\alpha/\text{Fe}]$ content and a significant contribution from the few high-mass systems accreted early on. Dwarf galaxies that survive until the present time were generally accreted later (within the last 5–6 Gyr) and had time to be enriched in Fe; hence their lower $[\alpha/\text{Fe}]$.

A slight modification to the simple “cosmic clock” picture (which includes the effect of mass) allows us to explain the high

⁵ Note that the Venn et al. (2004) data do not contain $[\text{O}/\text{Fe}]$; therefore we limit our comparison only to $[\text{Mg}/\text{Fe}]$.

⁶ The chemical abundance results shown throughout the paper are based on a modeling with the Kroupa initial mass function (IMF). However, we find that the choice of the IMF does not change significantly the results. Using a Salpeter IMF gives essentially the same abundance patterns and distribution functions. Note, however, that to obtain the same normalization discussed in § 2.2, the model with the Salpeter IMF requires less feedback or shorter star formation rate (see Robertson et al. [2005] for details).

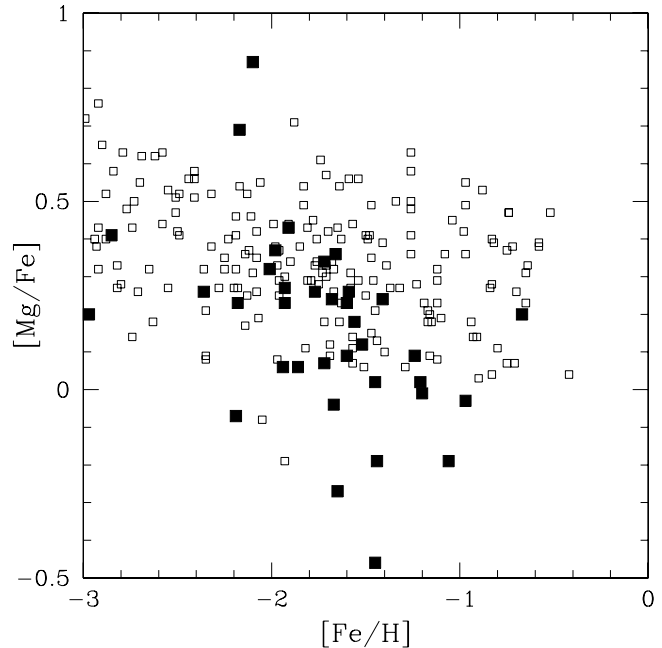


FIG. 8.— $[\text{Mg}/\text{Fe}]$ vs. $[\text{Fe}/\text{H}]$ for the Venn et al. (2004) compilation data. Open squares correspond to halo stars and filled squares to satellite stars. There are in total 36 satellite stars. For the halo, only the stars with halo membership probabilities greater than 50% are considered.

$[\text{Fe}/\text{H}]$ and/or high $[\alpha/\text{Fe}]$ component of the halo. In the framework of the hierarchical structure formation scenario, it is more appropriate to think of a multitude of “clocks” running at different rates and stopping at different times, associated with the individual star formation sites (i.e., progenitors of the halo). Most of these clocks are stopped either on or just after accretion of the satellites. Since the bulk of the halo formed from massive satellites accreted early, these had very efficient star formation and rapid enrichment to high $[\text{Fe}/\text{H}]$ (i.e., the cosmic clock in this case runs fast but stops early). In contrast, the dSphs had inefficient star formation and shut off at much later times.

Finally, this discrepancy in accretion times provides a natural explanation for the lack of a counterpart in the halo to the intermediate-age and young stellar populations seen in surviving satellites; the halo was in place sufficiently long ago (>8 Gyr) that it does not contain a significant number of such stars.

Overall, we have shown that once the full dynamics and chemical evolution are taken into account, the Λ CDM model can easily accommodate the chemical abundance patterns and stellar populations seen in the stellar halo and dSphs.

4.2. The Abundance Distribution Functions of the Milky Way

We note that the ADFs of our simulated data can only be cautiously compared with the available observations. Our ADFs (Figs. 6 and 7) are normalized functions over all stars in the local halo and surviving satellites, whereas the observational distributions are normalized functions only over a limited number of stars. For the stellar halo, the observational challenge is to select a truly random sample of stars. For the satellites, the current high-resolution spectral data is limited to a few stars each in some subset of the satellites, so it is impossible to construct a luminosity-weighted histogram.

Numerous MDFs have been derived for the Milky Way halo (Hartwick 1976; Laird et al. 1988; Ryan & Norris 1991; Carney et al. 1996; Chiba & Beers 2000). These studies have found that the peak of the halo MDF occurs around $[\text{Fe}/\text{H}] = -1.5$. In contrast,

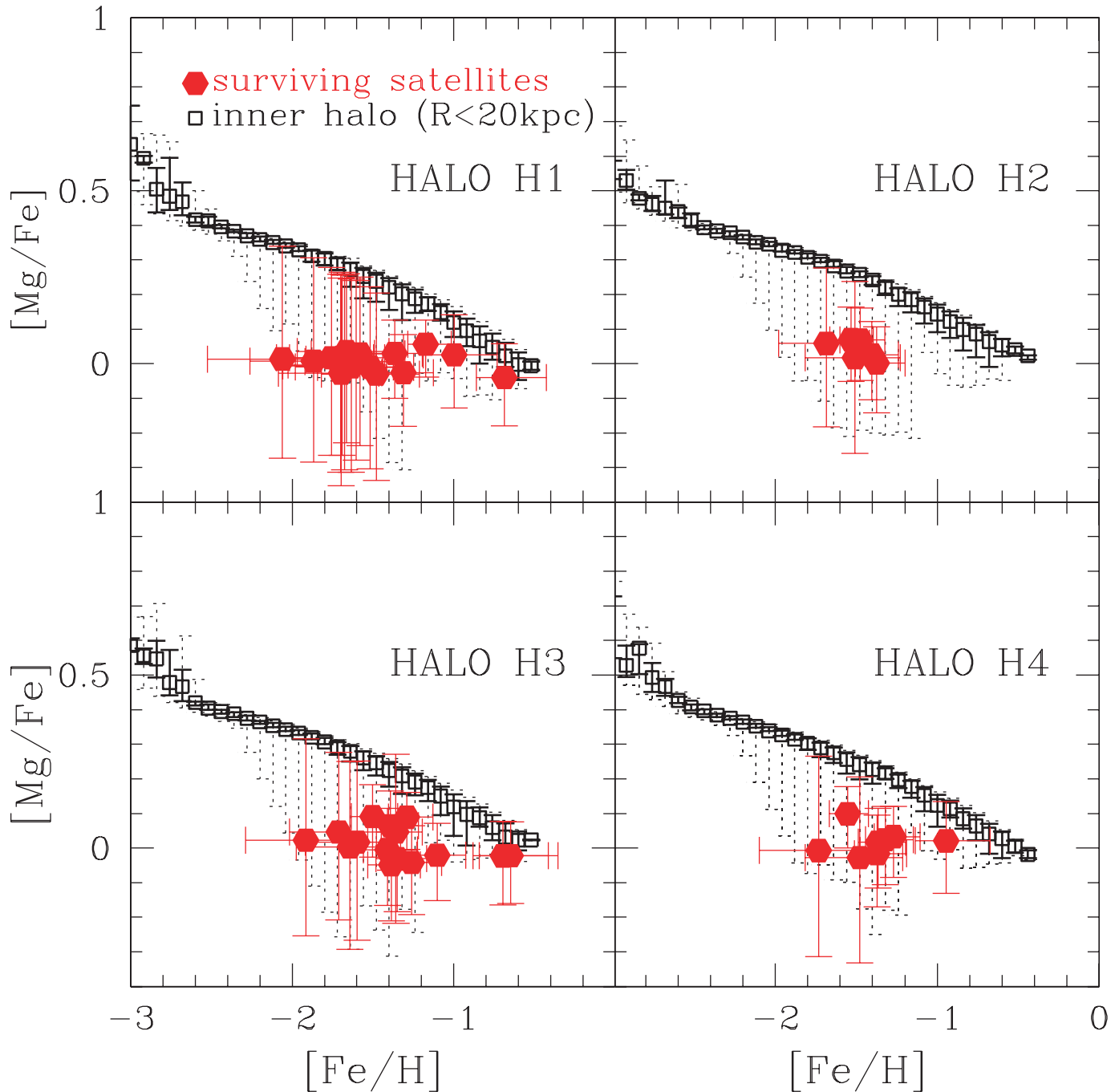


FIG. 9.— $[\text{Mg}/\text{Fe}]$ vs. $[\text{Fe}/\text{H}]$ for the sample of four halo simulations (values are weighted averages). Open squares correspond to inner halo ($R < 20$ kpc) values binned in $\Delta[\text{Fe}/\text{H}] = 0.1$ dex, and red hexagons correspond to values for surviving satellites. Solid lines represent error bars delineating 10% and 90% from the absolute spread in $[\text{Mg}/\text{Fe}]$ values. Dotted lines highlight the absolute extent in $[\text{Mg}/\text{Fe}]$ values for the inner halo.

metallicity data for dwarf galaxies in the Local Group (both satellites and in the field) are still sparse (see Grebel et al. 2003; Venn et al. 2004 and references therein), but recent and upcoming observations are aiming to bridge that gap (Kaufer et al. 2004; Tolstoy et al. 2004).

The top left panel in Figure 10 shows $[\text{Fe}/\text{H}]$ distributions based on a compilation of observational data, whereas the top right panel shows the $[\text{Mg}/\text{Fe}]$ distributions. The thick solid line corresponds to the sample of halo stars of Laird et al. (1988; note that this sample contains only $[\text{Fe}/\text{H}]$ data). The thin dashed lines plot the abundance distributions of satellite stars from the Venn et al. (2004) data. The available observational data seem to suggest

that the two $[\text{Fe}/\text{H}]$ distributions (halo and surviving satellite) have their peaks at about the same location, around -1.5 dex. In the Venn et al. (2004) data, the satellite stars' $[\text{Fe}/\text{H}]$ distribution seems to be narrower than that of the Milky Way halo, up to 1 dex. This is mainly because the Venn et al. (2004) satellite $[\text{Fe}/\text{H}]$ distribution seems to lack the very metal poor tail ($[\text{Fe}/\text{H}] \sim -4$ dex) seen in the corresponding halo stars' distribution. However, the Laird et al. (1988) halo data do not show the metal poor tail, and this sample is, unlike the Venn et al. (2004) data, unbiased in metallicity. Moreover, it is unclear whether the lack of metal-poor stars in Local Group dwarfs is real or just the result of incompleteness (at present there are only a few stars per satellite with measured

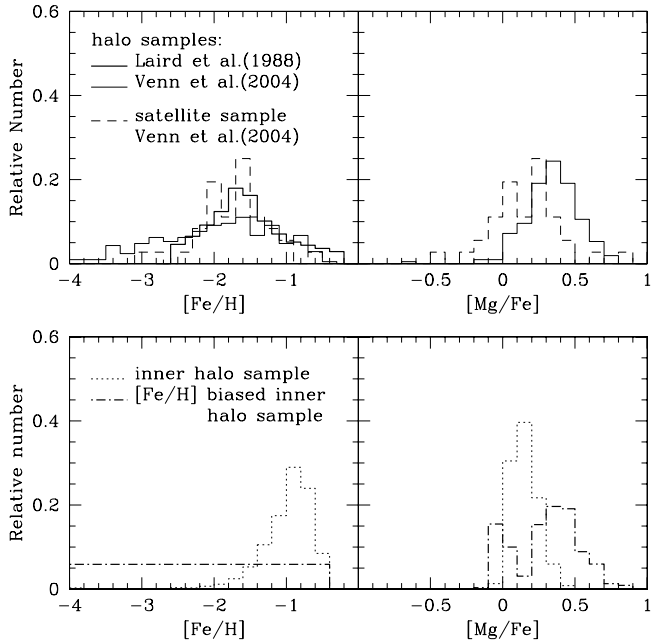


FIG. 10.—*Top panels:* $[\text{Fe}/\text{H}]$ distribution functions (*top left*) and $[\text{Mg}/\text{Fe}]$ distribution functions (*top right*) based on a compilation of observational data. The thick solid line corresponds to the sample of halo stars of Laird et al. (1988; note that this sample contains only $[\text{Fe}/\text{H}]$ data). Thin solid lines and dashed lines correspond to the ADFs of halo and satellite stars from the compilation data of Venn et al. (2004; see references therein for information about the original data). For the latter sample data, we consider only the stars whose halo membership probabilities are greater than 50%. *Bottom panels:* $[\text{Fe}/\text{H}]$ (*bottom left*) and $[\text{Mg}/\text{Fe}]$ (*bottom right*) distribution functions of stars in the inner H1 halo. Histograms represent relative number of stars normalized to the total number of stars in each sample. Dotted lines represent the entire collection of halo stars in the inner halo, whereas dot-dashed lines correspond to a biased selection of equal number of stars per $[\text{Fe}/\text{H}]$ bin.

chemical abundances). Stars in our model satellite galaxies also seem to have slightly lower $[\alpha/\text{Fe}]$ (see Figs. 9 and 7). This is in agreement with the observations (Fig. 10; Fig. 2 in Venn et al. 2004).

As discussed above, the Venn et al. (2004) sample contains an intrinsic bias toward selecting more metal-poor stars than in a random selection (the goal of their study was not to produce an MDF but to identify the $[\alpha/\text{Fe}]$ - $[\text{Fe}/\text{H}]$ correlation, which necessitates a rather uniform sampling of the $[\text{Fe}/\text{H}]$ range). Therefore the Venn et al. (2004) data are not appropriate for retrieving the halo $[\text{Fe}/\text{H}]$ distribution function. However, a bias in selecting $[\text{Fe}/\text{H}]$ does not necessarily translate into a bias in the $[\alpha/\text{Fe}]$. The $[\alpha/\text{Fe}]$ distribution function peaks are very narrow and unlikely to be missed by the Venn et al. (2004) study. We test this hypothesis by simulating a biased selection of halo stars of drawing from one of our simulated halos (halo H1) an equal number of stars in each $[\text{Fe}/\text{H}]$ bin and checking by what extent this choice affects the detection of the $[\alpha/\text{Fe}]$ distribution function peak (note that this case is more extreme than the selection of Venn et al. 2004). The bottom panels in Figure 10 show the resulting normalized histograms representing the $[\text{Fe}/\text{H}]$ and $[\text{Mg}/\text{Fe}]$ distribution functions of stars in the inner halo. Dotted lines represent the entire collection of inner halo stars and dot-dashed lines correspond to the biased selection (in total, the stars selected this way amount to less than 1% of the total stellar mass of the inner halo). The figure shows that even in this extreme case, the $[\text{Mg}/\text{Fe}]$ distribution function is remarkably close to the original one in retrieving the overdensity of stars with $[\text{Mg}/\text{Fe}] \sim 0$ – 0.5 values. This result gives us confidence that the ADF peak

revealed in the $[\text{Mg}/\text{Fe}]$ data of Venn et al. (2004) shows a real trend.

4.3. Differences in the ADFs of the Milky Way and M31

The Milky Way and M31 are two large spiral galaxies of similar size and mass but with significantly different metallicities. MDFs for different regions in the halo of M31 have been derived by a number of authors (Durrell et al. 2001; Reitzel & Guhathakurta 2002; Bellazzini et al. 2003; Durrell et al. 2004). The MDF peak of the M31 halo is located between $[\text{Fe}/\text{H}] \simeq -0.4$ and -0.7 , about 1 dex more metal-rich than that of the Milky Way halo (the range in different MDF peaks may indicate that observations probe regions with different substructure).

Our own results show that halos with the same mass and roughly the same stellar luminosity (e.g., halos H1 and H2) can have significantly different MDFs at the present time due to differences in their mass accretion histories. The $[\text{Fe}/\text{H}]$ peak of halo H2 is more metal rich ($[\text{Fe}/\text{H}] \simeq -0.6$) than that of halo H1 ($[\text{Fe}/\text{H}] \simeq -1$). As discussed before, both halos form at about the same time (see Fig. 1), however about 50% of the stellar mass of the inner H2 halo originates in one massive satellite ($M_* \sim 10^9 M_\odot$), whereas many smaller satellites make up the inner H1 halo (see Fig. 3). The more massive satellite in the H2 run has enriched the stellar halo with more metal-rich stars. Therefore, it is possible that M31 may have had one or a few more massive mergers than the Galaxy in the first few Gyr of its formation. Alternatively, a massive satellite accreted later and on very eccentric orbit (so as to decay rapidly) could have enriched the inner halo with more Fe. Indeed, such an accretion event seems to have been detected as a metal-rich, giant stellar stream (Ibata et al. 2001; Ferguson et al. 2002).

Moreover, the Milky Way MDF peak is ~ 0.5 dex more metal poor than the most metal poor of the four simulated halos analyzed here (halo H1), suggesting that the Galaxy could have formed mainly through accretion of smaller ($M_* < 10^9 M_\odot$) satellites. We note that the scatter at the high end of the mass spectrum can result in significant shifts in the MDF peaks; Figure 6 shows variations up to about 0.5 dex among halos. Interestingly, the only massive satellite known to be in an ongoing process of disruption, the Sagittarius galaxy, is expected to add a significant stellar mass enriched in $[\text{Fe}/\text{H}]$ to the halo in about 1–2 Gyr, and therefore to shift the MDF peak toward the more metal-rich end.

5. CONCLUSIONS

We have investigated the nature of the progenitors of the stellar halo for a set of Milky Way-type galaxies and studied the chemical enrichment patterns in the context of the Λ CDM model. The main results can be summarized as follows:

1. In the hierarchical scenario, stellar halos of Milky Way-type galaxies form inside out. The local halo (inner $R < 20$ kpc) assembles rapidly, with most of its mass already in place more than 8–9 Gyr ago. Satellites accreted more than 9 Gyr ago are completely disrupted by tidal forces. Satellites surviving today were accreted within the past few Gyr and fell in less-radial orbits. A significant portion (50%–80%) of present-day stellar halos is likely to have been originated in just a few massive satellites of $M_* \sim 10^8$ – $10^{10} M_\odot$.

2. Our model retrieves the chemical abundance patterns observed in the Galaxy (e.g., Venn et al. 2004). Our results show that differences between the accretion times and masses of surviving satellites versus the main progenitors of the local halo are a critical factor in determining the chemical abundance patterns. Surviving satellites have lower $[\alpha/\text{Fe}]$ than the progenitors of the

inner halo, because they have been accreted later, and Type Ia supernovae had enough time to enrich them with Fe. In contrast, the original building blocks were accreted fast (within the first few Gyr of the formation Galaxy) and contained stars enriched mainly by Type II supernovae. The local halo contains a significant population characterized by low [Fe/H] and high [α /Fe] ratios, originating in a few early accreted high-mass systems.

3. We also investigated the abundance distribution functions of both [Fe/H] and [α /Fe] ratios for stars in the halo and in surviving satellites and showed that the shapes and peaks of the distribution functions are directly related to the accretion history of the galaxies. We found a consistent shift between the peaks of the [α /Fe] distribution functions of stars in surviving satellites and those in the local halo. Surviving satellites have an [α /Fe] distribution peak near solar values, whereas that of the inner halo is typically around 0.1–0.2 dex.

We conclude that the difference in chemical abundance patterns in local halo versus surviving satellites arises naturally from the predictions of the hierarchical structure formation in a Λ CDM universe.

The chemical evolution model can be further improved by incorporating a more accurate treatment of the star formation history and of feedback mechanisms in the dwarf galaxy models (see Robertson et al. [2005] for a detailed discussion), or by modeling a larger number of chemical elements that can help constrain the merger history of the Galaxy (such as Ba, Y, and Eu). In addition, a number of refinements can be made in the dynamical evolution of the Galaxy models, such as modeling the interaction between satellites and other Galactic components or between the satellites themselves. While our model retrieves the main characteristics of the chemical abundance distributions in the Milky Way, improvements in both the chemical and dynamical modeling will enable more detailed comparisons with the observations.

A. F. would like to thank Falk Herwig, Kim Venn, and Ian McCarthy for useful discussions and suggestions. A. F. and K. V. J.'s contributions were supported through NASA grant NAG5-9064 and NSF CAREER award AST-0133617.

REFERENCES

- Bellazzini, M., et al. 2003, *A&A*, 405, 867
 Blumenthal, G. R., Faber, S. M., Primack, J. R., & Rees, M. J. 1984, *Nature*, 311, 517
 Brook, C. B., Gibson, B. K., Martel, H., & Kawata, D. 2005, *ApJ*, 630, 298
 Bullock, J. S., & Johnston, K. V. 2005, *ApJ*, 635, 931
 Buser, R. 2000, *Science*, 287, 69
 Carney, B. W., Laird, J. B., Latham, D. W., & Aguilar, L. A. 1996, *AJ*, 112, 668
 Chiba, M., & Beers, T. C. 2000, *AJ*, 119, 2843
 Côté, P., Marzke, R. O., West, M. J., & Minniti, D. 2000, *ApJ*, 533, 869
 Dekel, A., & Silk, J. 1986, *ApJ*, 303, 39
 Dekel, A., & Woo, J. 2003, *MNRAS*, 344, 1131
 Durrell, P. R., Harris, W. E., & Pritchett, C. P. 2001, *AJ*, 121, 2557
 ———. 2004, *AJ*, 128, 260
 Ferguson, A. M. N., Irwin, M. J., Ibata, R. A., Lewis, G. F., & Tanvir, N. R. 2002, *AJ*, 124, 1452
 Ferrara, A., & Tolstoy, E. 2000, *MNRAS*, 313, 291
 Freeman, K., & Bland-Hawthorn, J. 2002, *ARA&A*, 40, 487
 Fuhrmann, K. 1998, *A&A*, 338, 161
 Gallart, C., Freedman, W. L., Aparicio, A., Bertelli, G., & Chiosi, C. 1999, *AJ*, 118, 2245
 Gilmore, G., & Wyse, R. F. G. 1998, *AJ*, 116, 748
 Grebel, E. K., Gallagher, J. S., & Harbeck, D. 2003, *AJ*, 125, 1926
 Hartwick, F. D. A. 1976, *ApJ*, 209, 418
 Helmi, A., Navarro, J. F., Nordström, B., Holmberg, J., Abadi, M. G., & Steinmetz, M., 2006, *MNRAS*, submitted (astro-ph/0505401)
 Helmi, A., White, S. D. M., & Springel, V. 2003, *MNRAS*, 339, 834
 Ibata, R. A., Gilmore, G., & Irwin, M. J. 1994, *Nature*, 370, 194
 ———. 1995, *MNRAS*, 277, 781
 Ibata, R. A., Irwin, M. J., Ferguson, A. M. N., Lewis, G. F., & Tanvir, N. 2001, *Nature*, 412, 49
 Kaufer, A., Venn, K. A., Tolstoy, E., Pinte, C., & Kudritzki, R.-P. 2004, *AJ*, 127, 2723
 King, I. 1962, *AJ*, 67, 471
 Lacey, C., & Cole, S. 1993, *MNRAS*, 262, 627
 Laird, J. B., Carney, B. W., Rupen, M. P., & Latham, D. W. 1988, *AJ*, 96, 1908
 Larson, R. B. 1974, *MNRAS*, 169, 229
 Mac Low, M.-M., & Ferrara, A. 1999, *ApJ*, 513, 142
 Majewski, S. R. 1993, *ARA&A*, 31, 575
 Majewski, S. R., Munn, J. A., & Hawley, S. L. 1996, *ApJ*, 459, L73
 Majewski, S. R., et al. 2002, in *ASP Conf. Proc.* 285, *Modes of Star Formation and the Origin of Field Populations*, ed. E. K. Grebel & W. Brandner (San Francisco: ASP), 199
 Mateo, M. 1996, in *ASP Conf. Ser.* 92, *Formation of the Galactic Halo... Inside and Out*, ed. H. Morrison & A. Sarajedini (San Francisco: ASP), 434
 ———. 1998, *ARA&A*, 36, 435
 Matteucci, F. 2001, *The Chemical Evolution of the Galaxy* (Dordrecht: Kluwer)
 McWilliam, A. 1997, *ARA&A*, 35, 503
 Nissen, P. E., & Schuster, W. J. 1997, *A&A*, 326, 751
 Recchi, S., Matteucci, F., & D'Ercole, A. 2001, *MNRAS*, 322, 800
 Reitzel, D. B., & Guhathakurta, P. 2002, *AJ*, 124, 234
 Robertson, B., Bullock, J. S., Font, A. S., Johnston, K. V., & Hernquist, L., 2005, *ApJ*, 632, 872
 Ryan, S. G., & Norris, J. E. 1991, *AJ*, 101, 1835
 Searle, L. 1977, in *The Evolution of Galaxies and Stellar Populations*, ed. B. M. Tinsley & R. B. Larson (New Haven: Yale Univ. Press), 219
 Searle, L., & Zinn, R. 1978, *ApJ*, 225, 357
 Shetrone, M. D., Côté, P., & Sargent, W. L. W. 2001, *ApJ*, 548, 592
 Shetrone, M. D., Venn, K. A., Tolstoy, E., Primas, F., Hill, V., & Kaufer, A. 2003, *AJ*, 125, 684
 Smecker-Hane, T., & McWilliam, A. 1999, in *ASP Conf. Ser.* 192, *Spectro-Photometric Dating of Stars and Galaxies*, ed. I. Hubeny, S. R. Heap & R. H. Cornett (San Francisco: ASP), 150
 Somerville, R. S., & Kolatt, T. S. 1999, *MNRAS*, 305, 1
 Tolstoy, E., et al. 2004, *ApJ*, 617, L119
 Tosi, M., Steigman, G., Matteucci, F., & Chiappini, C. 1998, *ApJ*, 498, 226
 Unavane, M., Wyse, R. F. G., & Gilmore, G. 1996, *MNRAS*, 278, 727
 van den Bergh, S. 1994, *AJ*, 108, 2145
 Venn, K. A., Irwin, M., Shetrone, M. D., Tout, C. A., Hill, V., & Tolstoy, E. 2004, *AJ*, 128, 1177
 White, S. D. M., & Rees, M. 1978, *MNRAS*, 183, 341
 Wyse, R. F. G. 2001, in *ASP Conf. Ser.* 230, *Galactic Disks and Disk Galaxies*, ed. J. Funes & E. Corsini (San Francisco: ASP), 71
 Zentner, A. R., & Bullock, J. S. 2003, *ApJ*, 598, 49
 Zhao, D., Mo, H., Jing, Y. P., & Boerner, G. 2003, *MNRAS*, 339, 12